Natural Resources Canada
Ressources naturelles Canada

New constraints on the tectonothermal history of Southampton Island, Nunavut, provided by in situ SHRIMP geochronology and thermobarometry

R.G. Berman, N. Rayner, M. Sanborn-Barrie, and J. Chakungal

Geological Survey of Canada

Current Research 2011-6

2011

Canada

Geological Survey of Canada
Current Research 2011-6

New constraints on the tectonothermal history of Southampton Island, Nunavut, provided by in situ SHRIMP geochronology and thermobarometry

R.G. Berman, N. Rayner, M. Sanborn-Barrie, and J. Chakungal

2011

ISSN 1701-4387
Catalogue No. M44-2011/6E-PDF
ISBN 978-1-100-17575-1
doi:10.4095/287287

A copy of this publication is also available for reference in depository libraries across Canada through access to the Depository Services Program's Web site at http://dsp-psd.pwgsc.gc.ca

A free digital download of this publication is available from GeoPub: http://geopub.nrcan.gc.ca/index_e.php

Toll-free (Canada and U.S.A.): 1-888-252-4301

Recommended citation:
Berman, R.G., Rayner, N., Sanborn-Barrie, M., and Chakungal, J., 2011. New constraints on the tectonothermal history of Southampton Island, Nunavut, provided by in situ SHRIMP geochronology and thermobarometry; Geological Survey of Canada, Current Research 2011-6, 14 p. doi:10.4095/287287

Critical review
N. Wodicka

Authors
R.G. Berman (rberman@NRCan-RNCan.gc.ca)
N. Rayner (nrayner@NRCan-RNCan.gc.ca)
M. Sanborn-Barrie (msanborne@NRCan-RNCan.gc.ca)
Geological Survey of Canada
615 Booth Street
Ottawa, Ontario
K1A 0E9

J. Chakungal (joyia.chakungal@gov.yk.ca)
Yukon Geological Survey
2099 2nd Avenue
Whitehorse, Yukon
Y1A 1B5

Correction date:

New constraints on the tectonothermal history of Southampton Island, Nunavut, provided by in situ SHRIMP geochronology and thermobarometry

R.G. Berman, N. Rayner, M. Sanborn-Barrie, and J. Chakungal

Berman, R.G., Rayner, N., Sanborn-Barrie, M., and Chakungal, J., 2011. New constraints on the tectonothermal history of Southampton Island, Nunavut, provided by in situ SHRIMP geochronology and thermobarometry; Geological Survey of Canada, Current Research 2011-6, 14 p. doi:10.4095/287287

Abstract: Thermobarometry and in situ SHRIMP monazite geochronology reveal a complex, polycyclic history for Southampton Island, Nunavut. Two cryptic metamorphic events have been recognized at ca. 2.6 Ga (M_1) and 2.3 Ga (M_2) followed by four Paleoproterozoic events, some accompanied by deformation. Two samples on the western side of the study area record M_3-D_1 at 1879 ± 7 Ma and 1879 ± 8 Ma. Four samples constrain M_4-D_2 between 1861 ± 12 Ma and 1848 ± 6 Ma, with M_4 continuing to 1841 ± 4 Ma. Four samples also record a post-D_2, M_5 event between 1826 ± 9 Ma and 1815 ± 7 Ma, interpreted to represent a thermal culmination associated with extensive crustal melting and plutonism. Monazite growth between 1.79 Ga and 1.72 Ga likely reflects fluid ingress during cooling. These new data provide important constraints on the nature and timing of collisional events required to build robust tectonic and metallogenic models.

Résumé : La thermobarométrie et la géochronologie par datation *in situ* de la monazite à la microsonde SHRIMP révèlent une évolution polycyclique complexe de l'île Southampton, au Nunavut. Elles ont permis d'identifier deux épisodes métamorphiques cryptiques vers 2,6 Ga (M_1) et 2,3 Ga (M_2), suivis de quatre épisodes au Paléoprotérozoïque, dont certains accompagnés d'une déformation. Deux échantillons prélevés dans l'ouest de la région à l'étude révèlent un épisode de métamorphisme et de déformation M_3-D_1 à 1879 ± 7 Ma et à 1879 ± 8 Ma. Quatre échantillons circonscrivent chronologiquement l'épisode de métamorphisme et de déformation M_4-D_2 entre 1861 ± 12 et 1848 ± 6 Ma, avec un prolongement du métamorphisme M_4 jusqu'à 1841 ± 4 Ma. Quatre échantillons témoignent aussi d'un épisode de métamorphisme M_5 postérieur à la déformation D_2 entre 1826 ± 9 et 1815 ± 7 Ma, lequel, selon notre interprétation, représenterait un pic thermique associé à une fusion crustale à grande échelle et à une activité plutonique. La croissance de la monazite entre 1,79 et 1,72 Ga reflète probablement l'infiltration de fluides au cours du refroidissement. Ces nouvelles données fournissent des valeurs restrictives importantes sur la nature des épisodes de collision et le moment où ils se sont produits, des valeurs nécessaires à l'élaboration de modèles tectoniques et métallogéniques robustes.

INTRODUCTION

Situated within a 400 km wide gap between the mainland western Churchill Province and Baffin Island (Fig. 1), the geology of Southampton Island, Nunavut provides critical insight into the evolution of northeast Laurentia. Metamorphic studies initiated as part of the Southampton Island integrated geoscience project of the Northern Mineral Resources and Development Program constrain tectonic and regional metallogenic models, upon which exploration strategies for diamonds and precious- and base-metals in the area can be based. This report summarizes initial constraints on the pressure, temperature, and timing (P-T-t) of multiple metamorphic and deformation events on Southampton Island.

REGIONAL GEOLOGICAL SETTING

Located near the junction of five crustal blocks (Rae, Hearne, Chesterfield, Meta Incognita, and Sugluk; Fig. 1), the eastern half of Southampton Island exposes a highland of Precambrian rock comprising remnants of Archean psammite and semipelite, a potentially Paleoproterozoic carbonate-quartzite cover sequence, and voluminous plutonic rocks ranging from ultramafic (peridotite-dunite) to monzogranitic compositions (Sanborn-Barrie et al., 2008; Chakungal et al., 2008). Uranium-lead crystallization ages reveal extensive Archean (ca. 2.77–2.6 Ga) and Paleoproterozoic (ca. 1.94–1.82 Ga) magmatic activity (*see* Rayner et al., 2011), with Sm-Nd isotopic data (Whalen et al., 2011), supporting the presence of Meso- to Paleoarchean basement that correlates with Rae crust.

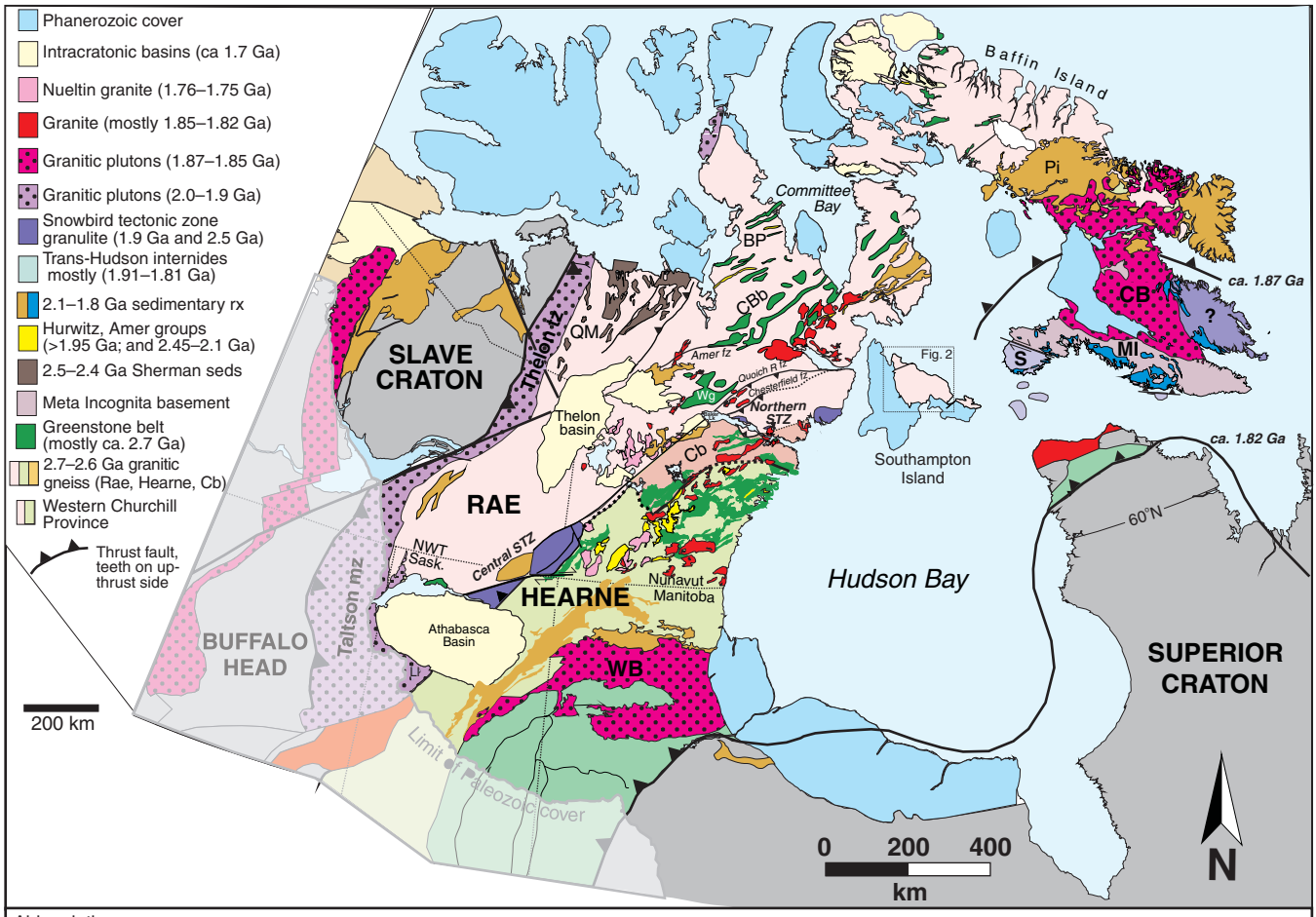

Abbreviations:
BP = Boothia Peninsula, Cb = Chesterfield block, Cbb = Committee Bay belt, CB = Cumberland Batholith, MI = Meta Incognita microcontinent, Pi = Piling, QM = Queen Maud, S = Sugluk block, STZ = Snowbird tectonic zone, WB = Wathaman Batholith, fz = fault zone.

Figure 1. Regional geology of the Precambrian core of Laurentia flanking Hudson Bay, modified from Berman et al. (2005).

Two penetrative deformational events are recognized in fabrics and structures observed throughout much of the study area. D_1 involves development of a moderately to steeply inclined, north-trending planar tectonic fabric (S_1) defined by high-grade mineral alignment and/or compositional layering. In metasedimentary rocks, S_1 is defined by aligned sillimanite, whereas orthopyroxene and biotite define S_1 in granodiorite (mangerite). During D_2, S_1 was strongly reworked into tight, recumbent, west-trending, south-vergent F_2 folds and/or relatively straight panels of gently inclined north- and west-striking S_1+S_2 transposition foliation. S_2 mineral assemblages indicate upper amphibolite- to granulite-facies conditions. Locally, broad, open, northeast-trending upright folds (F_3) of the transposition foliation highlight a nonpenetrative, near-horizontal component of shortening (D_3).

Quantitative metamorphic and geochronological constraints

In order to clarify the metamorphic evolution of the region, P–T conditions were estimated using the winTWQ software (version 2.35; Berman (2007)) following the methodology summarized by Berman et al. (2005). In order to link P-T conditions to timing constraints, six metasedimentary rock samples were chosen that contained monazite of a size (>10 μm) suitable for in situ SHRIMP analysis, carried out on 3 mm diameter cores drilled from texturally significant areas of polished thin sections with the methods of Rayner and Stern (2002). A small plug of pre-polished laboratory standard monazite (GSC monazite z3345 and z2908) was included on the mount. Stern and Berman (2000) described further analytical details. A Pb fractionation correction was applied to the Pb-isotope data in some instances (*see* Table 2 footnotes), the magnitude of which was determined by the analysis of monazite standards z3345 and z2908 the $^{207}Pb/^{206}Pb$ ages of which have been determined by isotope dilution methods (Stern and Berman, 2000). The error associated with the mass fractionation correction has been added quadratically to the isotopic ratios when calculating weighted mean ages. Common Pb correction utilized the Pb composition of the surface blank (Stern, 1997).

Table 1 summarizes thermobarometric and geochronological results for six, widely distributed samples (Fig. 2). Table 2 provides SHRIMP analytical data for monazite. Errors of mean ages and Concordia diagram ellipses are reported at 2σ. The geological context, textural relationships, thermobarometric data, and geochronological results for these six samples are presented below.

Sample 69HF-154a (GSC lab #8692)

Sample 69HF-154a is an archival sample from northern Southampton Island collected during reconnaissance mapping in 1969 (Heywood and Sanford, 1976). It is a garnet-sillimanite-biotite paragneiss in which garnet porphyroblasts are enveloped by a strong S_2 foliation defined by matrix biotite, sillimanite, and quartzofeldspathic shape fabric. The rim of one garnet porphyroblast hosts sillimanite inclusions that outline a folded or sheared S_1 fabric at an angle to S_2 (Fig. 3a). Ilmenite, quartz, and a monazite inclusion within the core of this garnet define a weak S_1 fabric that is subparallel to the sillimanite inclusion fabric (Fig. 3a), implying garnet growth during a progression from an early, weak S_1 fabric to a coarser grained S_1 fabric at higher grade. Most garnet porphyroblasts have inclusion-poor cores with syn-S_2 rims (not shown in Fig. 3) that are elongate parallel to S_2 and have overgrown S_2-aligned sillimanite and quartz inclusions.

Garnet cores are relatively calcic (X_{Ca} = 0.032–0.045) compared to syn-S_2 rims (X_{Ca} = 0.020–0.024). Both cores and rims have indistinguishable Fe/(Fe+Mg) between 0.71–0.72 and MnO between 0.5 and 0.6 weight per cent, probably indicating diffusive re-equilibration of the garnet core. Plagioclase is uniform in composition (X_{Ca} = 0.26–0.28), as is biotite (Fe/(Fe+Mg) = 0.32–0.34). Pressure-temperature conditions of 4.2 kbar and 630°C result from the rim compositions of garnet and biotite separated by quartz, and nearby plagioclase. The more calcic composition of the garnet core indicates its growth at higher pressure than garnet rims.

Five SHRIMP analyses of two monazite inclusions in the core of the garnet porphyroblast shown in Figure 3a yield a weighted mean $^{207}Pb/^{206}Pb$ age of 1879 ± 7 Ma (Mean Square of Weighted Deviates (MSWD) = 1.5; Fig. 3b). One of these grains is equant, whereas the other is elongate parallel to several nearby inclusions of ilmenite and quartz that define the early, weak S_1 fabric (Fig. 3a). A distinctly younger weighted mean $^{207}Pb/^{206}Pb$ age of 1841 ± 4 Ma (MSWD = 1.0; Fig. 3b) is derived from five analyses of three matrix grains interpreted as post-D_2 on the basis of their equant shapes.

Sample 07CYA-X64a (GSC lab #9477)

Sample 07CYA-X64a is a metaquartzite collected from a panel of calc-silicate-quartzite±semipelite, which was deposited after 2615 ± 23 Ma (Rayner et al., 2011) and, given the lithological association, may represent metasedimentary rocks correlative with Paleoproterozoic cover sequences on the Rae craton (Rainbird et al., 2010). The outcrop contains centimetre-sized porphyroblasts of garnet and cordierite, whereas the analyzed thin section contains the assemblage garnet-biotite-sillimanite-cordierite-K-feldspar-quartz-plagioclase-ilmenite. The outer parts of anhedral garnet porphyroblasts, up to 1 cm in diameter, contain a weak fabric (S_1, Fig. 4a, b) defined by the alignment of ilmenite, monazite, and sillimanite needles within one monazite inclusion (#241, inset of Fig. 4b). This internal S_1 foliation is at a high angle to the main (S_2) foliation, defined by elongate quartz and feldspar grains, that envelops the garnet (Fig. 4a).

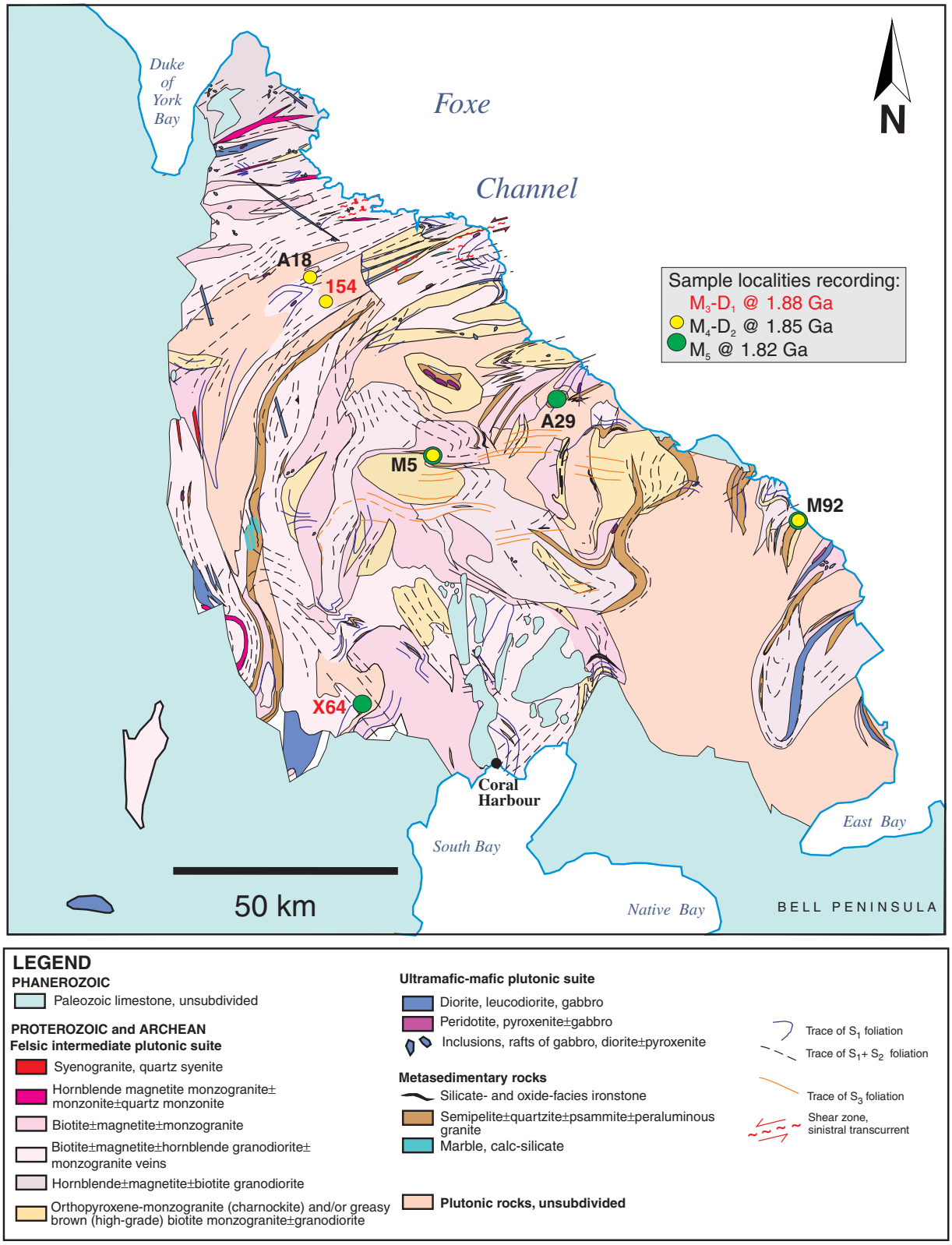

Figure 2. Simplified geology of Southampton Island (Sanborn-Barrie et al., 2008), with abbreviated sample numbers.

Table 1. Summary SHRIMP U-Pb in situ monazite ages and pressure-temperature conditions.

Sample #	Lithology	Age ± 2σ	Event	P-T estimates[1] T (°C)	P-T estimates[1] P(kbar)	Monazite textures
69HF-154a	Metapelite	1879 ± 7	M_3-D_1			S_1 garnet inclusions
		1841 ± 4	M_4	630^L	4.2^L	late M_4, post-D_2; equant matrix grains
07CYA-X64a	Metaquartzite	1879 ± 8	M_3-D_1			S_1 garnet inclusions
		1815 ± 7	M_5	755	7.4	post-D_2, equant matrix grain
		1790–1750	M_6			
07CYA-A18a	Metasemipelite	1849 ± 6	M_4-D_2	755	7.0	S_2 matrix grains and garnet inclusion
				655^P	6.6^P	
07CYA-M5	Metapelite	1866 ± 18	M_4-D_2			Garnet inclusion
		1826 ± 9	M_5			post-D_2, irregular matrix grains
07CYA-M92	Metasemipelite	1861 ± 12	M_4-D_2			S_2 matrix grain and garnet inclusion
		1820 ± 7	M_5	720	6.4	post-D_2, equant matrix grains
07CYA-A29	Metasemipelite	1816 ± 10	M_5	790	7.7	post-D_2, matrix grains and garnet inclusions
		1721 ± 36	M_6			

Errors are reported at the 2σ uncertainty level.
M_1, M_2 based on monazite ages from an S-type granite (Berman et al., unpub. data, 2010; Rayner et al., 2011).
[1]near-peak P-T conditions, except for: L = late, post-D_2 based on monazite textures, P = prograde; note that rims of garnet and matrix phases are assumed to have equilibrated during the last main monazite growth event recorded by each sample.

Garnet has a relatively uniform core composition, with X_{Ca} between 0.06–0.07, Fe/(Fe+Mg) = 0.69–0.72, and MnO decreasing slightly from 2.0 to 1.2 weight per cent toward the rim. The outer 50 µm of the garnet rim touching matrix K-feldspar has higher Fe/(Fe+Mg) up to 0.83, and lower X_{Ca} down to 0.033. This less calcic rim region has constant MnO (1.2 weight per cent) except for the extreme garnet rim (MnO = 2.0 weight per cent), indicating minor garnet resorption (e.g. Kohn and Spear, 2000).

Plagioclase forms mostly unzoned matrix grains (X_{An} = 0.24–0.26), although one matrix grain has a more sodic core (X_{An} = 0.18–0.21). More calcic (X_{An} = 0.30–0.38) plagioclase also forms about 20 µm wide discontinuous rims on quartz inclusions in garnet, with less calcic compositions generally in contact with garnet. The occurrence of plagioclase solely as rims between quartz inclusions and garnet indicates that plagioclase formed from garnet breakdown in the presence of a fluid which removed ferromagnesium components (no biotite is present in these inclusions). One 30 µm wide plagioclase inclusion in the garnet core has X_{An} = 0.35–0.42. In regions around plagioclase internal to garnet, garnet composition decreases from typical core X_{Ca} values to X_{Ca} = 0.030 (with Fe/(Fe+Mg) remaining low (0.69–0.70)). This decrease in X_{Ca} in garnet is also consistent with garnet breakdown to form plagioclase. Matrix biotite is unzoned with Fe/(Fe+Mg) = 0.49–0.51 and TiO_2 equals about 4 weight per cent. Biotite inclusions in garnet have low TiO_2 (2.6–3.2 weight per cent) and lower Fe/(Fe+Mg), ranging from 0.32 in contact with garnet to 0.35 in contact with quartz.

Pressure-temperature conditions of 7.4 kbar and 755°C were calculated from the rim compositions of garnet and biotite separated by matrix K-feldspar and nearby plagioclase. Cordierite could not be used because it is partially pinitized. The higher pressure conditions of garnet core formation (assumed from its more calcic composition) could not be calculated reliably, since plagioclase within garnet formed late in the history, and biotite within quartz inclusions in garnet appear to have re-equilibrated due to their contact with garnet.

The SHRIMP analyses of three aligned monazite inclusions in garnet (e.g. #241 in Fig. 4b inset) yielded a weighted mean $^{207}Pb/^{206}Pb$ age of 1879 ± 8 Ma (n = 5, MSWD = 0.42; Fig. 4c). Monazite inclusion #25, forming part of a weak internal fabric in another garnet porphyroblast, yielded an overlapping, but imprecise age (1896 ± 20 Ma, MSWD = 2.0) due to high ^{204}Pb. Six SHRIMP analyses of the near-rim, very low Y region of an equant, matrix grain (#1 in Table 2) yielded a weighted mean $^{207}Pb/^{206}Pb$ age of 1815 ± 7 Ma (MSWD = 0.92). Two analyses (#1.5 and 1.6) of the higher-Y core of this grain yielded a ca. 1.84 Ga

Table 2. SHRIMP U-Pb monazite results.

Spot name	Loc	U (ppm)	Th (ppm)	Th/U	Pb* (ppm)	^{204}Pb (ppb)	^{204}Pb/^{206}Pb	± ^{204}Pb/^{206}Pb	c f(206)^{204}	^{208*}Pb/^{206*}Pb	± ^{208}Pb/^{206}Pb	^{207*}Pb/^{235}U	± ^{207}Pb/^{235}U	^{206*}Pb/^{238}U	± ^{206}Pb/^{238}U	Corr Coeff	^{207*}Pb/^{206*}Pb	± ^{207}Pb/^{206}Pb	Apparent ages (Ma) ^{206}Pb/^{238}U	± ^{206}Pb/^{238}U	^{207}Pb/^{235}U	± ^{207}Pb/^{235}U	^{207}Pb/^{206}Pb	± ^{207}Pb/^{206}Pb	Conc. (%)
69HF-154a (UTM zone 17; 37147E, 7173550N)																									
8692-1.1	Grt-S_1	-	-	3.8	12344	332	5.92E-05	5.81E-06	0.0011	1.0702	0.0034	5.511	0.057	0.3482	0.0034	0.9683	0.1148	0.0003	1926	16	1902	9	1876	5	102.6
8692-1.1.2	Grt-S_1	-	-	3.9	11554	305	5.85E-05	4.02E-06	0.0011	1.0857	0.0041	5.388	0.059	0.3393	0.0035	0.9651	0.1152	0.0003	1883	17	1883	9	1882	5	100.1
8692-2.1	Grt-S_1	-	-	4.0	10361	289	6.32E-05	4.56E-06	0.0012	1.1349	0.0034	5.439	0.058	0.3403	0.0033	0.9352	0.1159	0.0004	1888	16	1891	9	1894	7	99.7
8692-2.2	Grt-S_1	-	-	4.2	11012	342	7.11E-05	3.62E-06	0.0013	1.1624	0.0043	5.533	0.056	0.3495	0.0034	0.9841	0.1148	0.0002	1932	16	1906	9	1877	3	103.0
8692-2.1.2	Grt-S_1	-	-	4.9	10136	288	7.13E-05	4.73E-06	0.0013	1.3745	0.0054	5.384	0.060	0.3404	0.0035	0.9598	0.1147	0.0004	1888	17	1882	10	1876	6	100.7
8692-7.1	Mat	-	-	4.1	7742	39	1.16E-05	2.54E-06	0.0002	1.1568	0.0066	5.352	0.054	0.3449	0.0033	0.9705	0.1125	0.0003	1910	16	1877	9	1841	4	103.8
8692-7.2	Mat	-	-	4.1	8276	39	1.09E-05	2.32E-06	0.0002	1.1530	0.0066	5.317	0.058	0.3437	0.0034	0.9425	0.1122	0.0004	1905	16	1872	9	1835	7	103.8
8692-8.1	Mat	-	-	9.2	8109	51	2.36E-05	3.56E-06	0.0004	2.6072	0.0116	5.157	0.053	0.3333	0.0032	0.9736	0.1122	0.0003	1854	16	1845	9	1836	4	101.0
8692-11.1	Mat	-	-	4.7	8099	34	1.04E-05	2.76E-06	0.0002	1.3429	0.0034	5.323	0.055	0.3419	0.0033	0.9619	0.1129	0.0003	1896	16	1873	9	1847	5	102.6
8692-11.2	Mat	-	-	4.5	8299	46	1.33E-05	2.58E-06	0.0003	1.2677	0.0033	5.328	0.058	0.3430	0.0036	0.9852	0.1127	0.0002	1901	17	1873	9	1843	3	103.2
07CYA-X64a (UTM zone 17; 361243E, 7124780N)																									
9477-240.1	Grt-S_1	5721	31060	5.4	7439	79	2.86E-05	4.27E-06	0.0004	1.5569	0.0049	5.365	0.099	0.3379	0.0061	0.9888	0.1152	0.0003	1876	29	1879	16	1882	5	99.7
9477-241.1	Grt-S_1	4763	25354	5.3	6004	72	3.17E-05	7.08E-06	0.0005	1.5247	0.0071	5.283	0.130	0.3316	0.0069	0.8961	0.1156	0.0013	1846	33	1866	21	1889	20	97.7
9477-241.2	Grt-S_1	6536	29893	4.6	7603	124	3.99E-05	6.11E-06	0.0006	1.3197	0.0139	5.256	0.106	0.3319	0.0065	0.9837	0.1149	0.0004	1848	31	1862	17	1878	7	98.4
9477-239.1	Grt-S_1	3089	30177	9.8	5773	69	4.74E-05	1.68E-05	0.0007	2.8143	0.0154	5.201	0.108	0.3299	0.0064	0.9665	0.1144	0.0006	1838	31	1853	17	1870	10	98.3
9477-239.2	Grt-S_1	3155	29976	9.5	5640	55	3.80E-05	7.18E-06	0.0006	2.7171	0.0572	5.126	0.127	0.3236	0.0075	0.9658	0.1149	0.0007	1807	37	1840	21	1878	12	96.2
9477-1.1	Mat	7297	32527	4.5	8237	44	1.28E-05	2.69E-06	0.0002	1.2942	0.0075	4.991	0.091	0.3260	0.0058	0.9867	0.1110	0.0003	1819	28	1818	15	1816	5	100.1
9477-1.2	Mat	5868	34142	5.8	7690	68	2.52E-05	5.52E-06	0.0004	1.6971	0.0057	4.979	0.096	0.3240	0.0060	0.9843	0.1115	0.0004	1809	29	1816	16	1823	6	99.2
9477-1.3	Mat	8695	37840	4.4	9280	62	1.60E-05	3.36E-06	0.0003	1.2607	0.0045	4.771	0.090	0.3127	0.0058	0.9876	0.1107	0.0003	1754	28	1780	16	1810	5	96.9
9477-1.4	Mat	6275	33915	5.4	7649	55	1.95E-05	4.25E-06	0.0003	1.5746	0.0053	4.820	0.092	0.3152	0.0058	0.9840	0.1109	0.0004	1766	29	1788	16	1815	6	97.3
9477-1.5	Mat	4252	59976	14.1	10281	55	2.81E-05	1.10E-05	0.0004	4.0838	0.0308	5.012	0.137	0.3224	0.0080	0.9464	0.1127	0.0010	1802	39	1821	23	1844	16	97.7
9477-1.6	Mat	9495	49697	5.2	11707	38	8.86E-06	8.16E-06	0.0001	1.5753	0.0099	4.928	0.098	0.3186	0.0061	0.9798	0.1122	0.0005	1783	30	1807	17	1835	7	97.1
9477-1.7	Mat	11589	29883	2.6	9216	43	8.78E-06	2.71E-06	0.0001	0.7508	0.0037	4.507	0.098	0.2973	0.0059	0.9484	0.1100	0.0008	1678	29	1732	18	1799	13	93.3
9477-1.8	Mat	10847	43076	4.0	10356	28	6.10E-06	3.91E-06	0.0001	1.1658	0.0047	4.468	0.095	0.2913	0.0058	0.9609	0.1112	0.0007	1648	29	1725	18	1820	11	90.6
9477-5.1	Mat	6340	35175	5.5	8142	123	4.16E-05	6.94E-06	0.0006	1.6275	0.0048	4.911	0.092	0.3258	0.0059	0.9863	0.1093	0.0003	1818	29	1804	16	1788	6	101.7
9477-5.2	Mat	3164	31150	9.8	5733	124	8.67E-05	2.09E-05	0.0013	2.8518	0.0183	4.680	0.095	0.3174	0.0061	0.9645	0.1069	0.0006	1777	30	1764	17	1748	10	101.7
9477-25.1	Grt-S_1	1399	28614	20.5	4741	481	7.61E-04	1.19E-04	0.0118	6.3905	0.0457	5.159	0.1685	0.3125	0.0079	0.8378	0.1197	0.0022	1753	39	1846	27	1952	32	89.8
9477-25.2	Grt-S_1	2176	32613	15.0	5487	801	7.70E-04	5.39E-05	0.0119	4.1623	0.0167	5.377	0.1559	0.3310	0.0087	0.9434	0.1178	0.0011	1843	42	1881	25	1923	17	95.8
9477-25.1.2	Grt-S_1	2476	48134	19.4	8001	381	3.24E-04	2.36E-05	0.0050	5.6458	0.0234	5.258	0.112	0.3311	0.0066	0.9678	0.1152	0.0006	1844	32	1862	18	1883	10	97.9
9477-25.3	Grt-S_1	2224	62422	28.1	10341	301	2.75E-04	3.12E-05	0.0043	8.2645	0.0474	5.465	0.157	0.3433	0.0090	0.9434	0.1155	0.0011	1902	43	1895	24	1887	17	100.8
9477-25.1.3	Grt-S_1	2342	52100	22.2	8383	215	1.99E-04	3.25E-05	0.0031	6.5795	0.0288	5.150	0.187	0.3222	0.0112	0.9751	0.1159	0.0009	1800	55	1844	30	1895	15	95.0
9477-25.1.4	Grt-S_1	2323	51670	22.2	8031	256	2.42E-04	3.57E-05	0.0038	6.4299	0.0585	5.036	0.116	0.3173	0.0063	0.9159	0.1151	0.0011	1777	31	1825	19	1881	17	94.4
9477-25.2.2	Grt-S_1	2269	36560	16.1	6432	308	2.84E-04	3.66E-05	0.0044	4.7720	0.0434	5.455	0.155	0.3334	0.0080	0.8930	0.1187	0.0015	1855	39	1894	24	1936	23	95.8
9477-25.4	Grt-S_1	2242	48110	21.5	7905	1580	1.42E-03	8.20E-05	0.0220	6.0470	0.0424	6.013	0.162	0.3403	0.0074	0.8680	0.1281	0.0017	1888	36	1978	23	2073	24	91.1
07CYA-A18a (UTM zone 16; 635346E, 7214885N)																									
9472-4.1	Grt-S_2	6569	61785	9.4	11730	237	7.74E-05	1.22E-05	0.0012	2.6906	0.0116	5.172	0.128	0.3254	0.0070	0.9175	0.1153	0.0011	1816	34	1848	21	1884	18	96.4
9472-4.2	Grt-S_2	7047	62390	8.9	12164	197	5.91E-05	1.42E-05	0.0009	2.5108	0.0164	5.156	0.122	0.3304	0.0073	0.9615	0.1132	0.0007	1840	35	1845	20	1851	12	99.4
9472-15.1	Mat-S_2	2309	37276	16.1	6248	181	1.68E-04	2.44E-05	0.0026	4.6178	0.0214	5.068	0.143	0.3272	0.0084	0.9441	0.1123	0.0011	1825	41	1831	24	1838	17	99.3
9472-14.1	Mat-S_2	2005	31152	15.5	5269	158	1.69E-04	1.89E-05	0.0026	4.4730	0.0291	5.092	0.158	0.3259	0.0094	0.9617	0.1133	0.0010	1819	46	1835	26	1853	15	98.1
9472-14.2	Mat-S_2	2452	40502	16.5	6568	181	1.65E-04	1.84E-05	0.0026	4.8194	0.0312	4.835	0.112	0.3129	0.0062	0.8998	0.1121	0.0011	1755	30	1791	19	1834	18	95.7
9472-14.3	Mat-S_2	2641	40986	15.5	6578	154	1.31E-04	3.36E-05	0.0020	4.4405	0.0286	4.820	0.147	0.3109	0.0089	0.9663	0.1124	0.0009	1745	44	1788	25	1839	14	94.9
9472-14.4	Mat-S_2	2824	43183	15.3	7701	333	2.42E-04	2.28E-05	0.0037	4.4478	0.0398	5.274	0.117	0.3399	0.0069	0.9494	0.1126	0.0008	1886	33	1865	19	1841	13	102.4
9472-19.1	Mat-S_2	1885	33352	17.7	5594	201	2.22E-04	2.01E-05	0.0034	5.0030	0.0210	5.251	0.124	0.3362	0.0074	0.9607	0.1133	0.0008	1868	36	1861	20	1853	12	100.8
9472-19.2	Mat-S_2	1779	45868	25.8	7123	178	2.19E-04	1.04E-04	0.0034	7.5810	0.0575	4.967	0.147	0.3189	0.0073	0.8340	0.1130	0.0019	1784	36	1814	25	1848	29	96.5
9472-19.3	Mat-S_2	2513	43125	17.2	6911	193	1.73E-04	1.92E-05	0.0027	5.0348	0.0463	4.852	0.141	0.3099	0.0074	0.8802	0.1136	0.0016	1740	37	1794	24	1857	25	93.7
9472-19.4	Mat-S_2	2247	48113	21.4	7594	197	1.92E-04	2.46E-05	0.0030	6.2173	0.0442	5.007	0.110	0.3193	0.0065	0.9535	0.1137	0.0008	1786	32	1820	18	1860	12	96.1
9472-19.5	Mat-S_2	2600	41005	15.8	7066	185	1.52E-04	1.76E-05	0.0024	4.6680	0.0390	5.109	0.221	0.3258	0.0133	0.9687	0.1138	0.0012	1818	65	1838	36	1860	19	97.7
9472-19.6	Mat-S_2	2649	43585	16.5	7087	209	1.76E-04	5.02E-05	0.0027	4.8107	0.0259	4.882	0.112	0.3129	0.0063	0.9237	0.1132	0.0010	1755	31	1799	19	1851	16	94.8
9472-19.7	Mat-S_2	2589	42539	16.4	6926	253	2.18E-04	2.03E-05	0.0034	4.8089	0.0189	4.800	0.140	0.3130	0.0086	0.9708	0.1112	0.0008	1756	42	1785	24	1819	13	96.5
9472-19.8	Mat-S_2	3143	50558	16.1	8197	208	1.51E-04	2.29E-05	0.0023	4.7706	0.0365	4.817	0.146	0.3071	0.0089	0.9764	0.1138	0.0008	1726	44	1788	25	1860	12	92.8
9472-19.9	Mat-S_2	2724	46026	16.9	7365	180	1.49E-04	1.80E-05	0.0023	4.9367	0.0390	4.860	0.121	0.3095	0.0071	0.9548	0.1139	0.0009	1738	35	1795	21	1862	13	93.4
9472-19.10	Mat-S_2	3304	55958	16.9	9260	285	1.91E-04	3.07E-05	0.0030	5.0284	0.0237	4.984	0.140	0.3161	0.0082	0.9530	0.1144	0.0010	1771	40	1817	23	1870	15	94.7
9472-3.1	Mat-S_2	3957	38455	9.7	7463	166	8.74E-05	9.57E-06	0.0014	2.7796	0.0166	5.224	0.108	0.3360	0.0065	0.9636	0.1128	0.0006	1867	32	1857	18	1845	10	101.2
9472-3.2	Mat-S_2	4579	44347	9.7	8279	191	9.05E-05	1.05E-05	0.0014	2.7852	0.0214	4.995	0.109	0.3217	0.0061	0.9151	0.1126	0.0010	1798	30	1818	18	1842	16	97.6
9472-3.3	Mat-S_2	4554	44467	9.8	8210	160	7.67E-05	9.51E-06	0.0012	2.7973	0.0180	4.959	0.100	0.3197	0.0060	0.9600	0.1125	0.0006	1788	29	1812	17	1840	10	97.2

Table 2. (cont.)

Spot name	Loc	U (ppm)	Th (ppm)	Th/U	Pb* (ppm)	^{204}Pb (ppb)	^{204}Pb/^{206}Pb	± ^{204}Pb/^{206}Pb	c f(206)^{204}	^{208*}Pb/^{206*}Pb	± ^{208}Pb/^{206}Pb	^{207*}Pb/^{235}U	± ^{207}Pb/^{235}U	^{206*}Pb/^{238}U	± ^{206}Pb/^{238}U	Corr Coeff	^{207*}Pb/^{206*}Pb	± ^{207}Pb/^{206}Pb	Apparent ages (Ma) ^{206}Pb/^{238}U	± ^{206}Pb/^{238}U	^{207}Pb/^{235}U	± ^{207}Pb/^{235}U	^{207}Pb/^{206}Pb	± ^{207}Pb/^{206}Pb	Conc. (%)
9472-3.4	Mat-S_2	4419	49343	11.2	8700	221	1.10E-04	2.44E-05	0.0017	3.1775	0.0146	4.912	0.286	0.3182	0.0182	0.9930	0.1119	0.0008	1781	90	1804	48	1831	12	97.3
9472-3.5	Mat-S_2	4783	55747	11.7	9765	273	1.25E-04	1.24E-05	0.0019	3.3134	0.0129	4.974	0.100	0.3198	0.0061	0.9756	0.1128	0.0005	1789	30	1815	17	1845	8	96.9
9472-3.6	Mat-S_2	6230	59839	9.6	10927	363	1.31E-04	1.42E-05	0.0020	2.8008	0.0213	4.846	0.127	0.3108	0.0078	0.9845	0.1131	0.0005	1744	39	1793	22	1850	8	94.3
9472-3.7	Mat-S_2	6430	60223	9.4	11351	226	7.74E-05	2.23E-05	0.0012	2.7322	0.0146	4.986	0.117	0.3183	0.0071	0.9786	0.1136	0.0006	1782	35	1817	20	1858	9	95.9
9472-3.8	Mat-S_2	5499	53622	9.8	9621	241	9.92E-05	1.10E-05	0.0015	2.8166	0.0279	4.790	0.109	0.3088	0.0064	0.9438	0.1125	0.0009	1735	31	1783	19	1840	14	94.3
07CYA-M5 (UTM zone 17; 375262E, 7179336N)																									
9475-20.1	Mat	3954	46978	11.9	7839	68	3.86E-05	6.93E-06	0.0006	3.2888	0.0348	4.806	0.113	0.3123	0.0067	0.9493	0.1116	0.0008	1752	33	1786	20	1826	13	96.0
9475-20.2	Mat	2013	46007	22.9	6778	97	1.10E-04	2.24E-05	0.0017	6.4843	0.0460	4.703	0.129	0.3070	0.0079	0.9611	0.1111	0.0009	1726	39	1768	23	1818	14	95.0
9475-20.3	Mat	2716	59686	22.0	8863	64	5.35E-05	1.70E-05	0.0008	6.1919	0.0369	4.717	0.117	0.3095	0.0070	0.9456	0.1105	0.0009	1738	35	1770	21	1808	15	96.1
9475-20.4	Mat	2404	54080	22.5	7384	70	7.20E-05	1.92E-05	0.0011	6.4513	0.0974	4.408	0.151	0.2812	0.0075	0.8409	0.1137	0.0021	1597	38	1714	28	1859	33	85.9
9475-20.5	Mat	2122	48112	22.7	6907	96	1.09E-04	5.66E-05	0.0017	6.6735	0.0652	4.542	0.198	0.2894	0.0079	0.7136	0.1138	0.0035	1639	40	1739	36	1861	55	88.0
9475-20.6	Mat	2241	51280	22.9	7168	112	1.20E-04	2.33E-05	0.0019	6.5416	0.0404	4.472	0.185	0.2895	0.0114	0.9747	0.1120	0.0010	1639	57	1726	34	1833	17	89.4
9475-20.7	Mat	2126	47868	22.5	6695	90	1.04E-04	2.05E-05	0.0016	6.5223	0.0342	4.434	0.105	0.2856	0.0061	0.9471	0.1126	0.0009	1620	31	1719	19	1842	14	87.9
9475-22.1	Mat	5552	47330	8.5	8967	58	2.32E-05	5.07E-06	0.0004	2.4591	0.0217	4.875	0.120	0.3137	0.0062	0.8650	0.1127	0.0014	1759	31	1798	21	1844	22	95.4
9475-22.2	Mat	4466	46601	10.4	8269	55	2.75E-05	9.34E-06	0.0004	3.0162	0.0248	4.819	0.116	0.3110	0.0067	0.9315	0.1124	0.0010	1745	33	1788	20	1838	16	94.9
9475-22.3	Mat	4461	44190	9.9	7989	65	3.25E-05	8.08E-06	0.0005	2.8754	0.0154	4.781	0.119	0.3115	0.0074	0.9708	0.1113	0.0007	1748	36	1781	21	1821	11	96.0
9475-22.4	Mat	4897	48271	9.9	8514	47	2.20E-05	6.76E-06	0.0003	2.8615	0.0211	4.693	0.126	0.3034	0.0078	0.9754	0.1122	0.0007	1708	39	1766	22	1835	11	93.1
9475-22.5	Mat	5646	51150	9.1	9078	76	3.12E-05	8.37E-06	0.0005	2.5814	0.0233	4.607	0.103	0.3021	0.0062	0.9481	0.1106	0.0008	1702	31	1751	18	1810	13	94.0
9475-22.6	Mat	6977	58191	8.3	10434	117	3.95E-05	1.13E-05	0.0006	2.3919	0.0180	4.556	0.115	0.2961	0.0068	0.9494	0.1116	0.0009	1672	34	1741	21	1826	14	91.6
9475-22.7	Mat	6194	55399	8.9	9536	66	2.58E-05	5.98E-06	0.0004	2.5548	0.0470	4.442	0.122	0.2914	0.0071	0.9307	0.1106	0.0011	1648	36	1720	23	1809	18	91.1
9475-22.8	Mat	4822	48448	10.0	7952	57	2.93E-05	7.97E-06	0.0005	2.9141	0.0232	4.386	0.114	0.2840	0.0065	0.9250	0.1120	0.0011	1611	33	1710	21	1832	18	88.0
9475-8.1	Grt	3521	32299	9.2	6283	66	3.96E-05	9.50E-06	0.0006	2.6147	0.0212	5.202	0.128	0.3320	0.0073	0.9360	0.1136	0.0010	1848	35	1853	21	1858	16	99.4
9475-8.1.2	Grt	3264	31668	9.7	6075	128	8.33E-05	1.61E-05	0.0013	2.8023	0.0268	5.198	0.108	0.3296	0.0063	0.9539	0.1144	0.0007	1836	31	1852	18	1870	11	98.2
07CYA-M92 (UTM zone 17; 462046E, 7143455N)																									
9476-12.1	Grt	2853	2087	0.7	1631	33	2.72E-05	9.92E-06	0.0004	0.2098	0.0056	4.562	0.102	0.3022	0.0065	0.9825	0.1095	0.0005	1702	32	1742	19	1791	8	95.0
9476-20.1	Grt-S_2	3561	28731	8.1	5820	72	4.28E-05	6.43E-06	0.0007	2.3113	0.0125	5.199	0.106	0.3311	0.0065	0.9830	0.1139	0.0004	1843	32	1852	17	1863	7	99.0
9476-20.2	Grt-S_2	3187	36686	11.5	6711	76	5.14E-05	9.32E-06	0.0008	3.4094	0.0366	5.079	0.135	0.3227	0.0074	0.9123	0.1142	0.0013	1803	36	1833	22	1867	20	96.6
9476-27.1	Mat-S_2	3036	31600	10.4	5814	41	2.95E-05	1.00E-05	0.0005	3.0247	0.0223	5.002	0.134	0.3209	0.0077	0.9344	0.1131	0.0011	1794	38	1820	22	1849	17	97.0
9476-6.1	Crd	3556	30648	8.6	6008	55	3.36E-05	6.82E-06	0.0005	2.5111	0.0091	4.981	0.096	0.3235	0.0060	0.9801	0.1117	0.0004	1807	29	1816	16	1827	7	98.9
9476-6.2	Crd	4678	30136	6.4	6413	18	8.58E-06	3.39E-06	0.0001	1.8862	0.0077	4.870	0.096	0.3174	0.0060	0.9825	0.1113	0.0004	1777	30	1797	16	1820	7	97.6
9476-6.3	Crd	2550	31452	12.3	5725	47	3.97E-05	2.04E-05	0.0006	3.7070	0.0219	5.001	0.141	0.3229	0.0078	0.9096	0.1123	0.0013	1804	38	1820	24	1838	21	98.2
9476-6.4	Crd	2176	27733	12.7	4846	36	3.57E-05	1.24E-05	0.0006	3.6995	0.0174	4.919	0.111	0.3209	0.0063	0.9228	0.1112	0.0010	1794	31	1805	19	1819	16	98.6
9476-6.5	Crd	4730	34816	7.4	6825	45	2.16E-05	7.80E-06	0.0003	2.1581	0.0097	4.701	0.102	0.3062	0.0060	0.9430	0.1113	0.0008	1722	30	1767	18	1821	13	94.5
9476-6.6	Crd	4541	33276	7.3	6741	41	2.00E-05	4.70E-06	0.0003	2.1394	0.0081	4.881	0.095	0.3168	0.0059	0.9814	0.1117	0.0004	1774	29	1799	16	1828	7	97.1
9476-6.7	Crd	2485	32372	13.0	5476	44	4.04E-05	9.88E-06	0.0006	3.8500	0.0245	4.682	0.098	0.3079	0.0061	0.9691	0.1103	0.0006	1730	30	1764	17	1804	9	95.9
9476-6.8	Crd	3551	34856	9.8	6188	63	4.11E-05	1.04E-05	0.0006	2.9060	0.0257	4.561	0.096	0.3009	0.0058	0.9574	0.1099	0.0007	1696	29	1742	17	1798	11	94.3
9476-6.9	Crd	4720	41765	8.8	7533	49	2.44E-05	6.96E-06	0.0004	2.6248	0.0237	4.546	0.108	0.2963	0.0062	0.9262	0.1113	0.0010	1673	31	1739	20	1820	16	91.9
9476-10.1	Mat	2631	30537	11.6	5626	66	5.26E-05	8.76E-06	0.0008	3.3079	0.0160	5.144	0.112	0.3355	0.0067	0.9518	0.1112	0.0008	1865	33	1843	18	1819	12	102.5
07CYA-A29 (UTM zone 17; 402370E, 7190263N)																									
9473-32.1	Mat	3514	59067	16.8	11069	59	3.24E-05	8.21E-06	0.0005	4.9105	0.0152	5.555	0.138	0.3624	0.0086	0.9763	0.1112	0.0006	1994	41	1909	21	1819	10	109.6
9473-32.2	Mat	3533	31035	8.8	6232	38	2.27E-05	6.73E-06	0.0004	2.5992	0.0122	5.050	0.105	0.3298	0.0065	0.9783	0.1111	0.0005	1837	32	1828	17	1817	8	101.1
9473-3.1	Mat	3161	23504	7.4	4733	33	2.27E-05	7.50E-06	0.0004	2.1542	0.0086	4.892	0.112	0.3182	0.0064	0.9184	0.1115	0.0010	1781	31	1801	19	1824	16	97.6
9473-3.2	Mat	3243	17883	5.5	3764	27	1.96E-05	9.93E-06	0.0003	1.5989	0.0113	4.593	0.117	0.2972	0.0070	0.9534	0.1121	0.0009	1678	35	1748	21	1833	14	91.5
9473-3.3	Mat	1752	2562	1.5	1083	22	3.14E-05	9.90E-06	0.0005	0.4082	0.0054	4.292	0.095	0.2836	0.0058	0.9554	0.1098	0.0007	1609	29	1692	18	1796	12	89.6
9473-10.1	Mat	1233	4225	3.4	1166	26	4.77E-05	1.53E-05	0.0007	0.9843	0.0107	4.569	0.119	0.3145	0.0072	0.9262	0.1054	0.0010	1763	36	1744	21	1721	18	102.4
9473-12.1	Grt	2456	4900	2.0	1850	4	4.09E-06	3.63E-06	0.0001	0.5801	0.0113	4.705	0.185	0.3101	0.0096	0.8523	0.1100	0.0023	1741	48	1768	32	1800	37	96.7

Notes (*see* Stern and Sanborn, 1998, Stern and Berman, 2000):
Spot name follows the convention x-y.z; where x = lab sample number, y = grain number, and z = spot number. Multiple analyses in an individual spot are labelled as x-y.z.z
Loc (monazite textural location): Mat = matrix grain; Crd, Grt = (cordierite, garnet) inclusions in host mineral; S_2 = aligned with S_2 fabric; S_1 = aligned with S_1 fabric
Uncertainties reported at 1σ (absolute) and are calculated by numerical propagation of all known sources of error
f206^{204} refers to mole fraction of total ^{206}Pb that is due to common Pb, calculated using the ^{204}Pb-method; common Pb composition used is the surface blank (4/6: 0.05770; 7/6: 0.89500; 8/6: 2.13840)
*Refers to radiogenic Pb (corrected for common Pb); concordance relative to origin = 100 * (^{206}Pb/^{238}Pb age)/(^{207}Pb/^{206}Pb age))
Calibration standard 3345; Age = 1821 Ma; ^{206}Pb/^{238}U = 0.32642
Analytical details:
IP363 (sample 8692): 16 µm spot, 6 scans; error in ^{206}Pb/^{238}U calibration 0.9%; no U concentration standard. No mass fractionation correction was applied.
IP458 (all samples except 8692): 16 µm spot, 5 scans; error in ^{206}Pb/^{238}U calibration 1.7%; U concentration standard 8153, 2065 ppm; Th/U calibration: F = 0.85700
Mass fractionation correction = +0.4% was applied to the Pb-isotope ratios.
Corr Coeff = correlation coefficient; Conc. = concordance

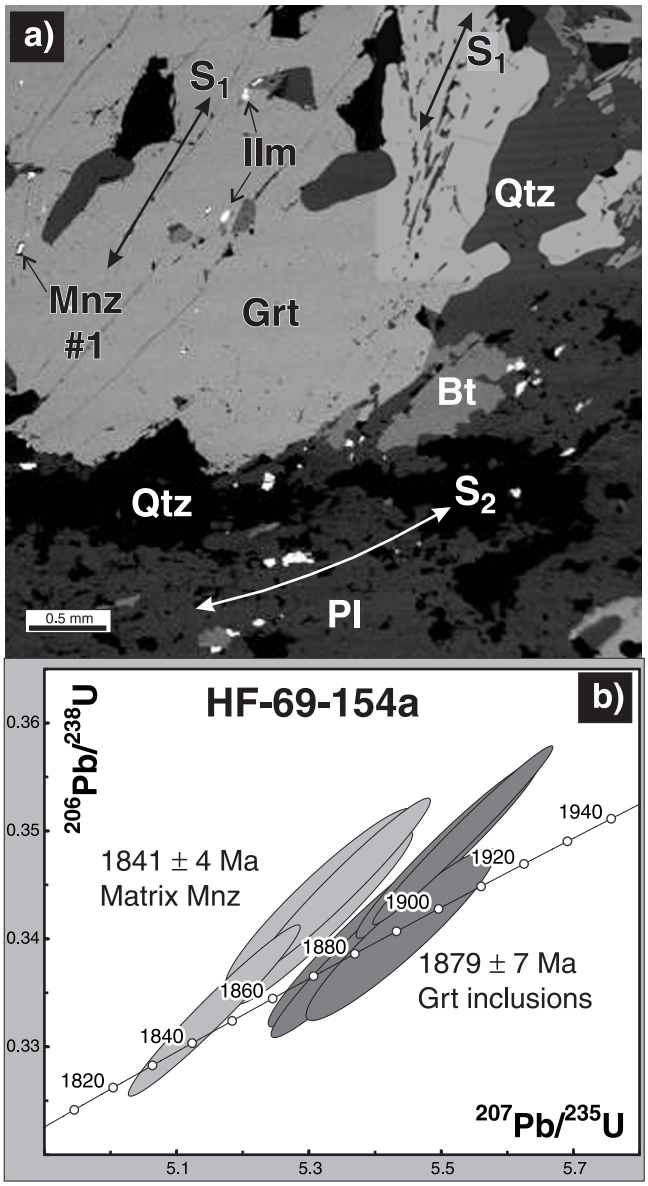

Figure 3. a) Backscattered scanning electron microscope image of textural relationships in sample 69HF-154a; note that right side of garnet is composite image showing sillimanite inclusion fabric (S_1); 2011-003; **b)** Concordia diagram of SHRIMP U-Pb results. Grt = garnet, Qtz = quartz, Ilm = ilmenite, Bt = biotite, Mnz = monzonite, Pl = plagioclase.

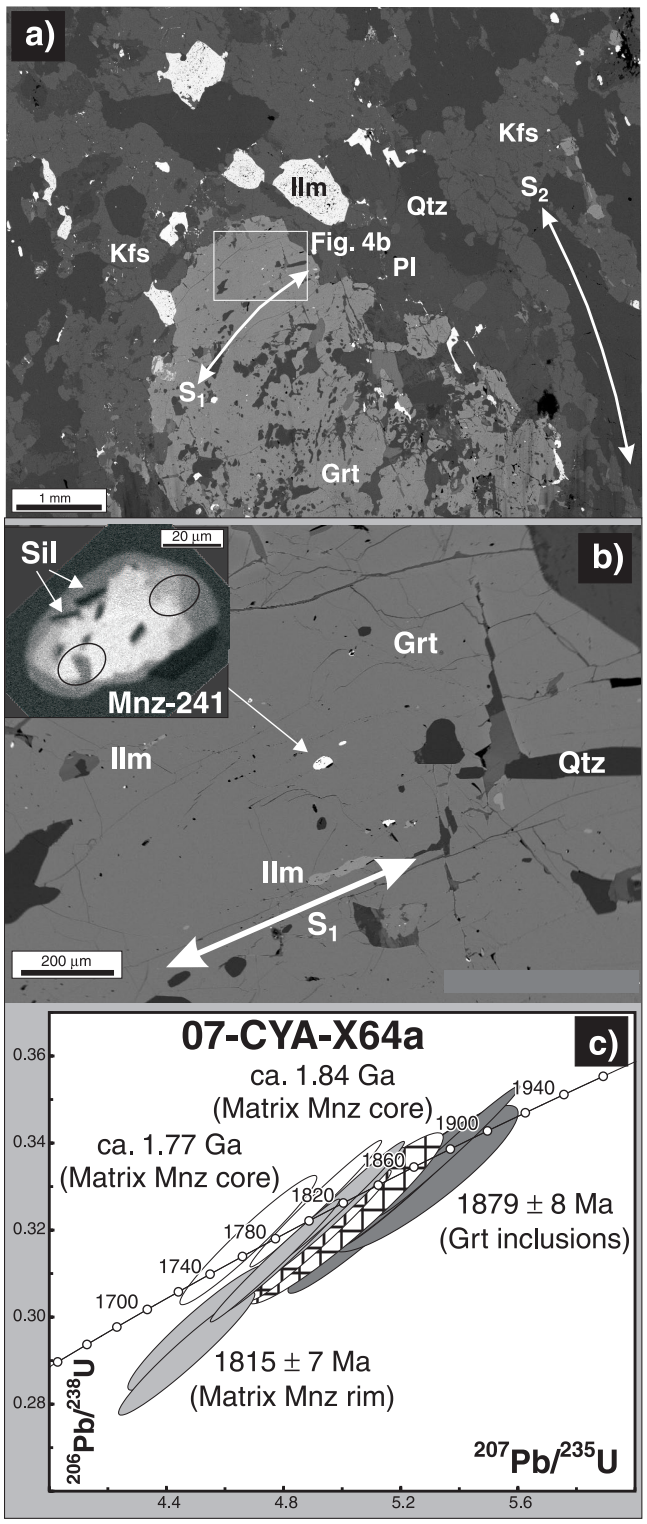

Figure 4. a), b) Backscattered scanning electron microscope image of textural relationships in 07CYA-X64a. Inset in (b) is Y map of analyzed monazite grain that is elongate parallel to weak internal S_1 fabric in garnet and which has overgrown S_1-parallel sillimanite needles; 2011-004, 2011-005. **c)** Concordia diagram of SHRIMP U-Pb results. Hatched ellipses are analyses of the core of a matrix monazite. Grt = garnet, Ilm = ilmenite, Qtz = quartz, Kfs = K-feldspar, Sil = sillimanite, Mnz = monazite.

age. The older of these two analyses (#1.5) has distinctly higher Th/U ratio (14.1) than all other analyses (Th/U <6), suggesting that the core of this monazite grain crystallized during an earlier, ca. 1.84 Ga event than the rim. One small matrix grain that is not aligned with the S_2 foliation yields two disparate ca. 1.77 Ga results (grain #5, Table 2).

Sample 07CYA-A18a (GSC lab #9472)

Sample 07CYA-A18a is a metapsammite with the assemblage garnet-orthopyroxene-cordierite-sillimanite-biotite-K-feldspar-plagioclase-quartz-ilmenite collected from an outcrop with visible orthopyroxene and some leucosome. The single strong foliation at this outcrop is oriented at 336/36°NE. It is interpreted as the regional S_2 foliation that has been deflected from the typical southwest-strike (e.g. 260/29°N) observed several kilometres to the northeast at station 07CYA-A19. In sample 07CYA-A18a, garnet porphyroblasts up to 1 cm in diameter are equant, variably embayed, and wrapped by the main foliation (S_2) defined by elongate grains of quartz, K-feldspar, and cordierite (Fig. 5a). The largest garnet contains small ilmenite and rutile needles that are parallel to S_2 (Fig. 5a), whereas smaller garnet porphyroblasts contain randomly oriented inclusions of quartz and plagioclase. Sparse, S_2-parallel sillimanite is intergrown with matrix cordierite, commonly in areas with relict, Zn-bearing spinel. Sparse biotite forms scattered matrix grains.

Garnet has uniform Fe/(Fe+Mg) between 0.60 and 0.61, except for an increase up to 0.64 at rims touching cordierite. Garnet cores are calcic (X_{Ca} = 0.06–0.08), decreasing to 0.046–0.049 at rims touching matrix plagioclase or quartz and at the location of plagioclase inclusions. No zoning in MnO is discernible. Matrix plagioclase is uniform in composition (X_{Ca} = 0.40–0.42). Plagioclase inclusions in garnet have sodic cores (X_{Ca} = 0.32–0.35) that increase to more calcic rims (up to X_{Ca} = 0.49) in contact with garnet. Matrix biotite varies in Fe/(Fe+Mg) between 0.35 and 0.37, with TiO_2 between 6.2–6.6 weight per cent. One biotite inclusion partly surrounded by plagioclase in garnet has Fe/(Fe+Mg) = 0.21–0.22 and TiO_2 = 2.0–2.5 weight per cent, suggesting that it crystallized at lower grade than matrix biotite. Cordierite forming partial rims on garnet is uniform in composition.

The compositions of randomly oriented plagioclase and biotite inclusions in garnet (Grt-1, Fig. 5a), together with calcic garnet near these inclusions yield pressure and temperature conditions of 6.6 kbar and 655°C, interpreted to represent prograde conditions prior to the onset of D_2. Pressure and temperature conditions of 7 kbar and 755°C result from the rim compositions of garnet touching cordierite, together with nearby biotite and plagioclase.

The weighted average $^{207}Pb/^{206}Pb$ age of 23 analyses from 4 low-Y, elongate, S_2-parallel matrix monazite grains (i.e. Mnz-3; Fig. 5b), is 1848 ± 6 Ma (MSWD = 0.78; Fig. 5c).

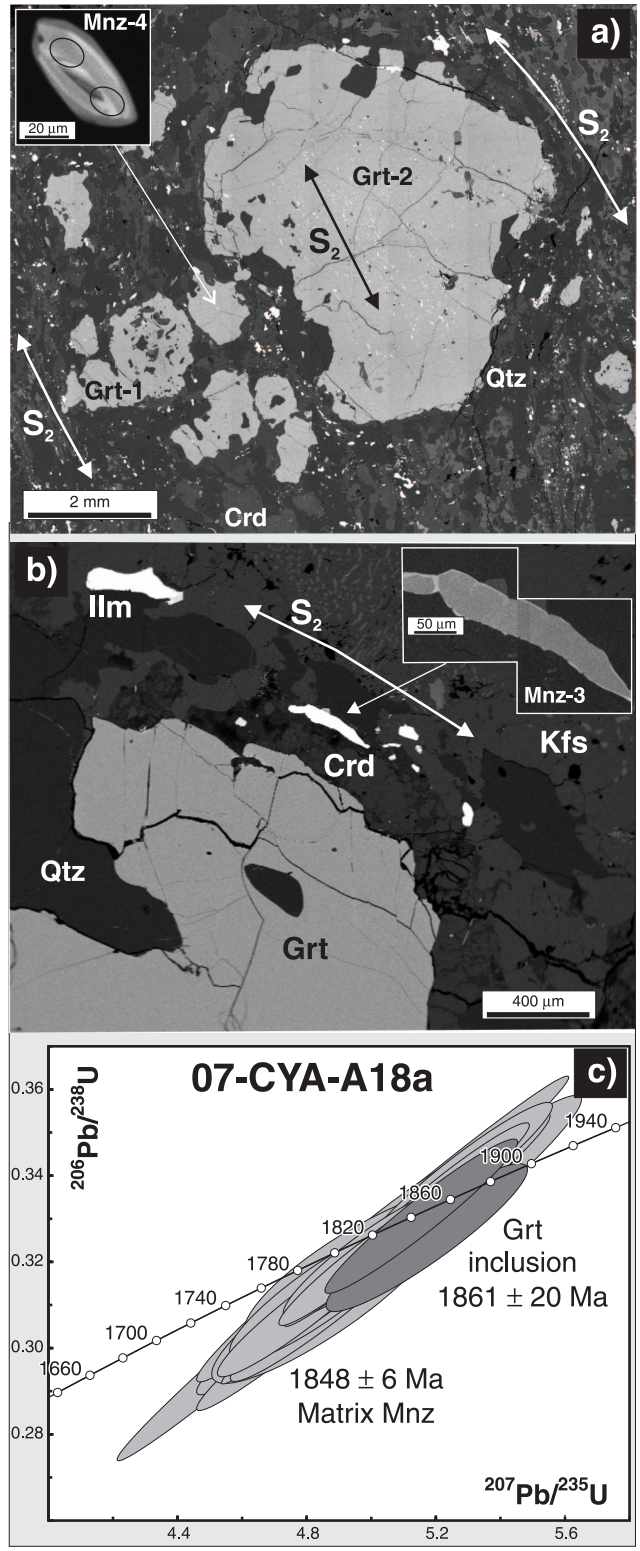

Figure 5. a) Backscattered scanning electron microscope image of textural relationships in sample 07CYA-A18a. Inset is Y map of analyzed monazite grain. **b)** Backscattered scanning electron microscope image of elongate matrix monazite parallel to S_2. Inset is composite Y map of analyzed monazite grain; 2011-006, 2011-007. **c)** Concordia diagram illustrating SHRIMP U-Pb results. Grt = garnet, Qtz = quartz, Crd = cordierite, Ilm = ilmenite, Kfs = K-feldspar, Mnz = monazite.

Two analyses of an S_2-parallel, monazite inclusion (Mnz-4, Fig. 5a) within garnet (Grt-2, Fig. 5a) possibly indicate an older component (ca. 1.86 Ga); however, this is not statistically distinguishable from the age of matrix monazite in this sample. The weighted mean age of all 25 monazite analyses (matrix and inclusion) is 1849 ± 6 Ma (MSWD = 0.89).

Sample 07CYA-M5 (GSC lab #9475)

This sample was collected from garnet-rich metapelite that forms rare, 2–10 cm wide layers within poorly exposed metaquartzite felsenmeer. Large (centimetre diameter), embayed garnet porphyroblasts are wrapped by the main foliation defined by coarse sillimanite needles and a preferred shape fabric in quartz and K-feldspar. Plagioclase is not present in this sample, which prevents calculation of pressure-temperature conditions.

Fifteen analyses from two, moderate-Y monazite grains that occur along the edge of a garnet porphyroblast (Fig. 6a) yield an average $^{207}Pb/^{206}Pb$ age of 1826 ± 9 Ma (MSWD = 0.68, Fig. 6b). Two analyses of a small, moderate-Y monazite inclusion in garnet yield a weighted mean $^{207}Pb/^{206}Pb$ age of 1866 ± 18 Ma (MSWD = 0.38, Fig. 6b).

Sample 07CYA-M92 (GSC lab #9476)

This sample from a raft of rusty metapelite included within diorite near the eastern coast of Southampton Island contains the assemblage garnet-biotite-cordierite-sillimanite-plagioclase-quartz. Garnet forms centimetre-sized, variably embayed porphyroblasts that are wrapped by a strong external fabric (S_2) defined by biotite, quartz, and feldspar (Fig. 7a). The cores of some garnet porphyroblasts contain inclusions of quartz and biotite that form a moderate internal fabric that is parallel to the external S_2 fabric. Some garnet has 0.3 mm wide rims of cordierite with minor quartz.

Inclusion-rich garnet cores are more calcic (X_{Ca} = 0.065–0.086) than clear rims (X_{Ca} = 0.041), with relatively uniform Fe/(Fe+Mg) between 0.70–0.72. The slight enrichment in MnO of garnet rims (1.0 weight per cent) relative to cores (0.75–0.80 weight per cent) likely occurred during partial breakdown of rims to cordierite. The Fe/(Fe+Mg) of matrix biotite near garnet, but surrounded by quartz increases from 0.4 to 0.45 with proximity to garnet, and is considered to reflect Fe enrichment during partial garnet breakdown (e.g. Kohn and Spear, 2000). Pressure and temperature conditions of 6.4 kbar and 720°C (with garnet-cordierite and garnet-biotite Fe-Mg exchange temperatures agreeing within 20°C) were calculated from the compositions of garnet just inside the MnO-enriched rim, biotite furthest removed from garnet, cordierite adjacent to garnet, and matrix plagioclase. Lack of appropriate inclusions in garnet preclude calculation of the conditions of garnet core formation.

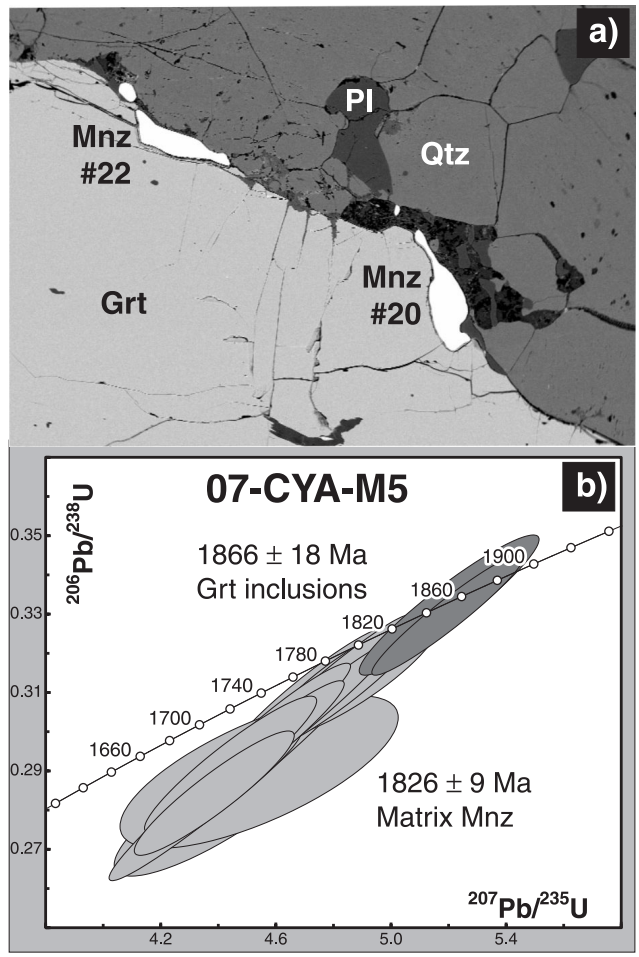

Figure 6. a) Backscattered scanning electron microscope image of textural relationships in sample 07CYA-M5; 2011-008. **b)** Concordia diagram illustrating SHRIMP U-Pb results. Grt = garnet, Qtz = quartz, Mnz = monazite.

Two SHRIMP analyses of a S_2-aligned, moderate- to high-Y monazite inclusion (#20) in garnet and one analysis of a small, S_2-parallel, moderate-Y, matrix grain (#27) yield a weighted mean $^{207}Pb/^{206}Pb$ age of 1861 ± 12 Ma (MSWD = 0.31, Fig. 7b). Nine analyses of equant, low-Y matrix grain #6 (Fig. 7b), which has a thin, very high-Y, unanalyzed rim, and one analysis of a small matrix grain (#10) that lies at a high angle to S_2, yield a weighted mean $^{207}Pb/^{206}Pb$ age of 1820 ± 7 Ma (MSWD = 1.08, Fig. 7b). A small monazite inclusion in garnet (#12) that is intersected by a large fracture gave a $^{207}Pb/^{206}Pb$ age of 1791 ± 16 Ma (2σ), interpreted as a mixed age based on the distinct Y zonation in Mnz-12 parallel to this fracture.

Sample 07CYA-A29 (GSC lab #9473)

Sample 07CYA-A29 is a granulite-facies metapsammite (Fig. 2) with the assemblage garnet-orthopyroxene-biotite-K-feldspar-plagioclase-quartz-ilmenite. Irregular, embayed garnet porphyroblasts up to 7 mm in diameter are wrapped

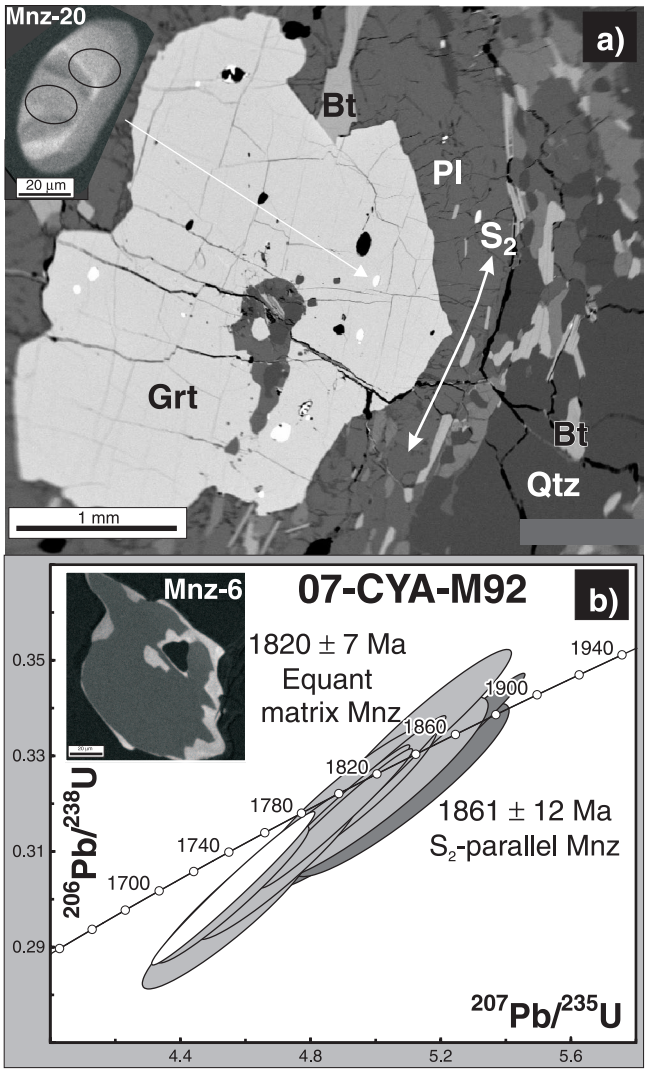

Figure 7. a) Backscattered scanning electron microscope image of textural relationships in sample 07CYA-M92. Inset shows Y map of analyzed monazite inclusion in garnet; 2011-009. **b)** Concordia diagram illustrating SHRIMP U-Pb results. Inset shows Y map of equant monazite grain with high-Y undated rim. Grt = garnet, Bt = biotite, Qtz = quartz, Pl = plagioclase, Mnz = monazite.

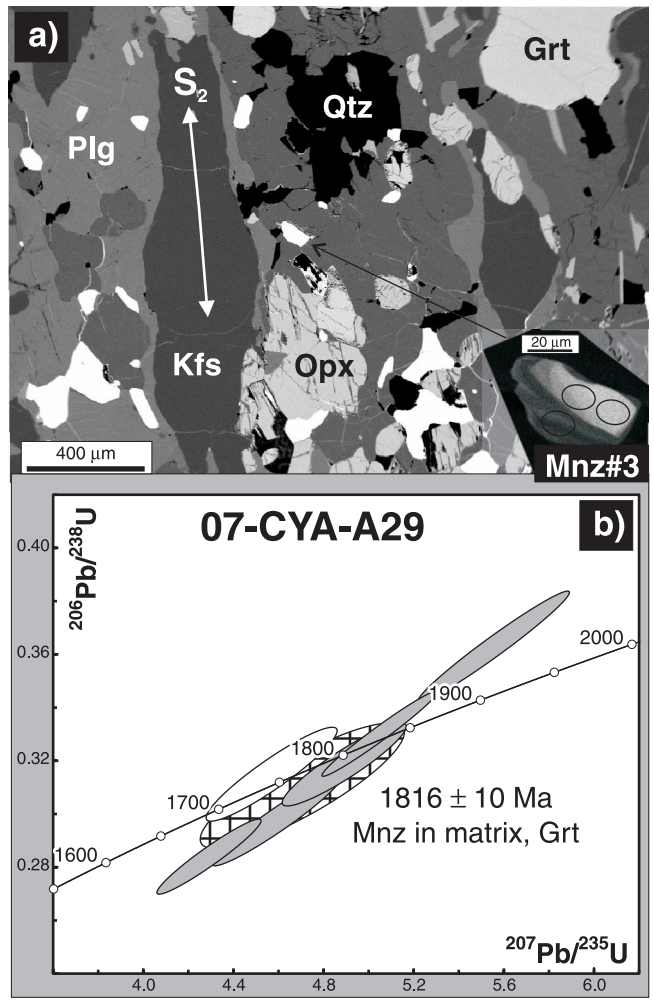

Figure 8. a) Backscattered scanning electron microscope image of textural relationships in sample 07CYA-A29. Inset shows Y map of monazite #3; 2011-010 **b)** Concordia diagram illustrating SHRIMP U-Pb results. Hatched ellipse is analysis of monazite inclusion in garnet. Grt = garnet, Qtz = quartz, Pl = plagioclase, Opx = orthopyroxene, Kfs = K-feldspar, Mnz = monazite.

by the main foliation (S_2) defined by alignment of biotite, orthopyroxene, and ilmenite with the preferred shape of quartz and feldspar (Fig. 8a). Smaller, relict garnet is surrounded and in places replaced by biotite.

Garnet porphyroblasts have texturally indistinct calcic core regions (X_{Ca} = 0.14–0.17) surrounded by less calcic regions and rims (X_{Ca} = 0.093–0.102). The Fe/(Fe+Mg) and MnO are uniform (0.73–0.74 and 0.9–1.0 weight per cent, respectively), except for relict garnet, which has higher Fe/(Fe+Mg) and MnO (0.76–0.78, and 1.2 weight per cent, respectively). Plagioclase is very consistent in composition (X_{Ca} = 0.38–0.42), except where it is adjacent to relict garnet (X_{Ca} = 0.48). Also relatively uniform in composition are orthopyroxene (Fe/(Fe+Mg) = 0.48–0.51; Al_2O_3 = 1.4–1.7 weight per cent) and biotite (Fe/(Fe+Mg) = 0.43–0.45, TiO_2 = 5.1–5.3 weight per cent). Pressure-temperature conditions of 7.7 kbar and 790°C result from rim compositions of garnet separated from orthopyroxene and biotite by plagioclase.

Six analyses, from two matrix grains and one inclusion in garnet, yield a weighted mean $^{207}Pb/^{206}Pb$ age of 1816 ± 10 Ma (MSWD = 0.99, Fig. 8b). One of these matrix grains (#3) is at a high angle to S_2 (Fig. 8a), whereas the other (#32) is a stubby grain (2:1 aspect ratio) parallel to S_2. A discrete, low-Th rim of grain #3 gives a nominally younger age (1796 ± 24 Ma, Fig. 8b) that nevertheless is statistically indistinguishable from the mean. One analysis of monazite (#10) within biotite adjacent to relict garnet gives a much younger age, 1721 ± 36 Ma, interpreted as dating this garnet breakdown reaction.

DISCUSSION

The quantitative metamorphic and geochronological data presented above provide first-order constraints on the tectonometamorphic evolution of Southampton Island, with evidence for four distinct metamorphic events and two penetrative deformational events. The nomenclature used below for these events (Table 1) is predicated on evidence of M_1 at ca. 2.6 Ga and M_2 at ca. 2.3 Ga, as derived from preliminary monazite data (Berman et al., unpub. data, 2010) for a ca. 2.68 Ga S-type granite (Rayner et al., 2011).

M_3-D_1 at 1.88 Ga

Samples 07CYA-X64a and 69HF-154a both display a weak first generation (S_1) foliation within garnet that is oriented at a high angle to the main S_2 foliation. In both samples, elongate monazite inclusions contribute to S_1, and yield near-identical 1879 ± 7 Ma and 1879 ± 8 Ma ages for M_3 at an early stage of D_1 deformation. The occurrence of monazite within the calcic cores of garnet in both samples indicates that M_3-D_1 occurred at relatively high pressure, strengthening a potential link with the Chesterfield block to the west (Fig. 1), where 7–10 kbar pressures are recorded at ca. 1.89–1.88 Ga (Berman et al., 2007). The 1.88 Ga event is considered to reflect microcontinent accretion to the Rae craton during an early stage of Hudsonian Orogeny (Berman et al., 2005, 2007). At present the 1.88 Ga event is evident only in two samples on west side of the study area (Fig. 2). Further studies are underway to determine the areal extent of this event on Southampton Island, and should better constrain the tectonic boundary conditions of this event.

M_4-D_2 at 1.86–1.84 Ga

Four samples widely distributed across Southampton Island record evidence for a 1.86–1.84 Ga event (Fig. 2). Monazite inclusions in garnet form a texturally distinct population of high-Y grains in three samples (07CYA-M5, 07CYA-A18a, and 07CYA-M92). The nominally older age of these inclusions in two of the samples (1866 ± 18 Ma and 1861 ± 20 Ma for 07CYA-M5 and 07CYA -A18a, respectively) are similar to the 1861 ± 12 Ma age of S_2-aligned matrix monazite and garnet inclusions in sample M92, suggesting that they may date the early stages of D_2 deformation and M_4 garnet growth. Elongate matrix monazite grains in sample 07CYA-A18a record a slightly younger age of 1848 ± 6 Ma. Equant matrix monazite in sample 69HF-154a may indicate that D_2 had ended in the north by 1841 ± 4 Ma, whereas S_2-foliated 1852 ± 8 Ma granodiorite and 1842 ± 5 Ma diorite (Rayner et al., 2011) establish that D_2 was ongoing across the south until at least ca. 1840 Ma. The occurrence of only syn-M_4-D_2 monazite in sample 07CYA-A18a suggests that the calculated pressure-temperature values for this sample (6.6 kbar and 655°C and 7 kbar and 755°C, Table 1) constrain a clockwise pressure-temperature-time path for the M_4 event.

The M_4-D_2 event at 1.86–1.84 Ga overlaps with the 1852 ± 6 Ma age of granodiorite plutonism on Southampton Island (Rayner et al., 2011). Given the strong penetrative deformation characterizing this event, the clockwise pressure-temperature path determined for sample 07CYA-18a, the monazite evidence that this event began prior to 1852 Ma, and the geochemistry of 1852 Ma granodiorite (Whalen et al., 2011), M_4-D_2 is consistent with a collisional event involving crustal thickening. This collisional event is also believed to have resulted in northwest-vergent folding and thickening that induced 1.86–1.84 Ga monazite growth further northwest in the Committee Bay belt (Berman et al., 2005). Crustal thickening at this time may have been driven by the ca. 1.88–1.86 Ga collision of Meta Incognita microcontinent with the southeastern flank of the Rae craton (St-Onge et al., 2006; Berman et al., 2005).

M_5 at 1.82 Ga

Four samples across Southampton Island (07CYA-M5, 07CYA-M92, 07CYA-A29, 07CYA-X64a) record evidence of an M_5 event, with statistically indistinguishable ages, ranging from 1826 ± 9 Ma to 1815 ± 7 Ma (Table 1). In agreement with the 1822 ± 3 Ma age of a late- to post-tectonic monzogranite (Rayner et al., in 2011), the M_5 event is interpreted as post-D_2 based on textural evidence that all monazite (except for #32 in CYA-07-A29; *see* above) is either equant in shape, or elongate at a high angle to the S_2 fabric. The extremely low-Y content of most of the 1.82 Ga grains (e.g. Fig. 7b inset) suggests a high-grade event during which garnet was stable, rather than releasing yttrium during breakdown. Pressure-temperature conditions for this event are consistent with this interpretation, with results calculated from rim compositions in three samples ranging between 6.4 kbar and 720°C and 7.7 kbar and 790°C (Table 1).

The M_5 event is similar in age to a metamorphic event dated on southwest Baffin Island (Rayner et al., 2008), and appears to represent a regional thermal culmination associated with voluminous crustal melting and plutonism dated at 1.83–1.82 Ga on Southampton Island and southwest Baffin Island (Rayner et al., 2008, 2011).

M_6 at ca. 1.79–1.72 Ga

Monazite growth at this time is recorded in sample 07CYA-A29, where 1.72 Ga monazite is associated with garnet breakdown, and in 07CYA-X64a, where a single, post-D_2 matrix grain ranges in age between 1.79 Ga and 1.75 Ga. The authors interpret these ages to reflect fluid influx during regional cooling.

CONCLUSIONS

Thermobarometric and in situ SHRIMP monazite geochronology provide the first constraints on Southampton Island's metamorphic and deformational history which are required to improve regional tectonic and metallogenic models. The new data reveal a complex, polycyclic evolution with the possibility of six metamorphic and two penetrative deformational events. Preliminary monazite ages from ca. 2.68 Ga S-type granite suggest M_1 at ca. 2.6 Ga and M_2 at 2.3 Ga (Berman et al., unpub. data, 2010). Monazite inclusions in garnet from two samples on the western side of the study area define M_3-D_1 at ca. 1880 Ma, which may mark an early accretionary event in the region. M_4-D_2, initiated by 1861 ± 12 Ma with garnet growth, and continued until at least 1848 ± 6 Ma. Equant matrix monazite in one sample suggests that post-D_2, M_4 metamorphism affected the northern part of exposed basement at 1841 ± 4 Ma, whereas deformation continued across the south until at least 1842 ± 5 Ma. The timing of the M_4-D_2 event is consistent with age constraints on Baffin Island (St-Onge et al., 2007) for the accretion of Meta Incognita microcontinent to the southeastern flank of the Rae Province. Four samples also record a post-D_2, M_5 event between 1826 ± 9 Ma and 1815 ± 7 Ma, which is interpreted to represent a thermal culmination associated with extensive crustal melting and ca. 1.83–1.82 Ga post-D_2 plutonism (Rayner et al., 2011). Monazite ages of ca. 1.79 Ga and 1.72 Ga may correspond to fluid influxes during regional cooling.

ACKNOWLEDGMENTS

This project was funded by the GSC's Northern Mineral Resources and Development Program, the Canada-Nunavut Geoscience Office, and Polar Continental Shelf Program. D. James contributed to the authors' understanding of the study area through discussions and field interpretations. The authors thank P. Hunt, T. Pestaj, and K. Venance for assistance with acquiring SEM, SHRIMP, and microprobe data, respectively. A constructive review of this paper by N. Wodicka is greatly appreciated.

REFERENCES

Berman, R.G., 2007. winTWQ (version 2.3): A Microsoft Windows-compatible software package for performing internally-consistent thermobarometric calculations; Geological Survey of Canada, Open File 5462, 41 p. doi:10.4095/223425

Berman, R.G., Sanborn-Barrie, M., Stern, R.A., and Carson, C.J., 2005. Tectonometamorphism at ca. 2.35 and 1.85 Ga in the Rae Domain, western Churchill Province, Nunavut, Canada; insights from structural, metamorphic and *in situ* geochronological analysis of the southwestern Committee Bay Belt; Canadian Mineralogist, v. 43, p. 409–442. doi:10.2113/gscanmin.43.1.409

Berman, R.G., Davis, W.J., and Pehrsson, S., 2007. The collisional Snowbird tectonic zone resurrected: growth of Laurentia during the 1.9 Ga accretionary phase of the Trans-Hudson orogeny; Geology, v. 35, p. 911–914. doi:10.1130/G23771A.1

Chakungal, J., Sanborn-Barrie, M., James, D., Rayner, N., Whalen, J., Craven, J., Spratt, J., Kosar, K., Ross, M., Zhang, S., and Coyle, M.. 2008. Natural resource potential – yes or no? Southampton Island Integrated Project: a summary of 2007 & 2008 results and investigations; *in* 36th Annual Yellowknife Geoscience Forum Abstracts, v. 36, p. 66.

Heywood, W.W. and Sanford, B.V., 1976. Geology of Southampton, Coats, and Mansel islands, District of Keewatin, Northwest Territories; Geological Survey of Canada, Memoir 382, 35 p.

Kohn, M.J. and Spear, F., 2000. Retrograde net transfer reaction insurance for pressure-temperature estimates; Geology, v. 28, p. 1127–1130. doi:10.1130/0091-7613(2000)28<1127:RNTRIF>2.0.CO;2

Rainbird, R., Davis, W., Pehrsson, S., Wodicka, N., Rayner, N., and Skulski, T., 2010. Early Paleoproterozoic supracrustal assemblages of the Rae domain, Nunavut, Canada: intracratonic basin development during supercontinent break-up and assembly; Precambrian Research, v. 181, p. 167–186. doi:10.1016/j.precamres.2010.06.005

Rayner, N. and Stern, R.A., 2002. Improved sample preparation method for SHRIMP analysis of delicate mineral grains exposed in thin sections; Geological Survey of Canada, Current Research, v. 2002-F10, 3 p. doi:10.4095/213626

Rayner, N.M., St-Onge, M.R., Berman, R.G., Sanborn-Barrie, M., and Wodicka, N., 2008. Polyphase tectonometamorphic history in the upper plate of Trans-Hudson Orogen (southern Baffin Island); Geochimica et Cosmochimica Acta, v. 72, p. A780.

Rayner, N., Chakungal, J. and Sanborn-Barrie, M., 2011. New U-Pb geochronological results from plutonic and sedimentary rocks of Southampton Island, Nunavut; Geological Survey of Canada, Current Research 2011-5. doi:10.4095/287286

Sanborn-Barrie, M., Chakungal, J., James, D., Whalen, J., Rayner, N., Berman, R.G., Craven, J., and Coyle, M., 2008. New understanding of the geology and diamond prospectivity of Southampton Island, central Nunavut; *in* 36th Annual Yellowknife Geoscience Forum Abstracts, v. 36, p. 53.

St-Onge, M.R., Searle, M.P., and Wodicka, N., 2006. Trans-Hudson Orogen of North America and Himalaya-Karakoram-Tibetan Orogen of Asia; structural and thermal characteristics of the lower and upper plates; Tectonics, v. 25, cit. no. TC4006. doi:10.1029/2005TC001907

St-Onge, M.R., Wodicka, N., and Ijewliw, O., 2007. Polymetamorphic evolution of the Trans-Hudson Orogen, Baffin Island, Canada: integration of petrological, structural and geochronological data; Journal of Petrology, v. 48, p. 271–302. doi:10.1093/petrology/egl060

Stern, R.A., 1997. The GSC Sensitive High Resolution Ion Microprobe (SHRIMP): analytical techniques of zircon U-Th-Pb age determinations and performance evaluation; Geological Survey of Canada, Current Research 1997-F, 31 p.

Stern, R.A. and Berman, R.G., 2000. Monazite U-Pb and Th-Pb geochronology by ion microprobe, with an application to *in situ* dating of an Archean metasedimentary rock; Chemical Geology, v. 172, p. 113–130. doi:10.1016/S0009-2541(00)00239-4

Stern, R.A. and Sanborn, N., 1998. Monazite U-Pb and Th-Ph geochronology by high-resolution secondary ion mass spectrometry; Geological Survey of Canada, Current Research 1998-F, 18 p.

Whalen, J.B., Sanborn-Barrie, M., and Chakungal, J., 2011. Geochemical and Nd isotopic constraints from plutonic rocks on the magmatic and crustal evolution of Southampton Island, Nunavut; Geological Survey of Canada, Current Research 2011-2, 14 p. doi:10.4095/286319

Geological Survey of Canada Project TG7002